Electronic Supplementary Material to: Impacts of Aerosol–Radiation Interactions on the Wintertime Particulate Pollution under Different Synoptic Patterns in the Guanzhong Basin, China*

Naifang BEI[1], Xia LI[2], Qiyuan WANG[2], Suixin LIU[2], Jiarui WU[2], Jiayi LIANG[1], Lang LIU[2], Ruonan WANG[2], and Guohui LI[2,3]

[1]*School of Human Settlements and Civil Engineering*, *Xi'an Jiaotong University*, *Xi'an* 710049, *China*

[2]*Key Laboratory of Aerosol Chemistry and Physics*, *State Key Laboratory of Loess and Quaternary Geology*, *Institute of Earth Environment*, *Chinese Academy of Sciences*, *Xi'an* 710061, *China*

[3]*Center for Excellence in Quaternary Science and Global Change*, *Chinese Academy of Sciences*, *Xi'an* 710061, *China*

ESM to: Bei, N. F., and Coauthors, 2021: Impacts of aerosol–radiation interactions on the wintertime particulate pollution under different synoptic patterns in the Guanzhong Basin, China. *Adv. Atmos. Sci.*, **38**(7), 1141–1152, https://doi.org/10.1007/s00376-020-0329-7.

Model Validations

Figure S1 presents the distributions of predicted and observed near-surface mass concentrations of $PM_{2.5}$, O_3, NO_2, and SO_2 along with the simulated wind fields averaged during the simulated episode. Generally, the predicted spatial pattern of $PM_{2.5}$ is consistent with observations at ambient monitoring sites in the GZB. The WRF-Chem model reasonably reproduces the high $PM_{2.5}$ concentrations exceeding 150 μg m^{-3} in the central GZB. Apparently, during the simulation period, the weak winds in the GZB facilitate accumulation of air pollutants, causing heavy PM pollution. The observed and simulated O_3 concentrations are rather low in the GZB, particularly regarding the area with high $PM_{2.5}$ levels, varying from 10 to 50 μg m^{-3}. There are several reasons for the low O_3 concentrations in the GZB during wintertime. Firstly, the weak insolation in northern China in winter is unfavorable for O_3 photochemical production. Additionally, high $PM_{2.5}$ concentrations and frequent occurrence of clouds during haze days further attenuate the incoming solar radiation in the planetary boundary layer (PBL), decreasing the O_3 levels. Secondly, weak winds indicate stagnant situations, lacking the O_3 transport from outside of the GZB. Thirdly, high NO_x emissions cause titration of O_3, which is shown by the high NO_2 concentrations in the central GZB. The elevated NO_2 concentrations are observed and simulated in the GZB, particularly in cities and their surrounding areas, ranging from 20 to 70 μg m^{-3}. The near-surface SO_2 concentrations in the GZB do not exceed 30 μg m^{-3} during the study period, which is mainly due to implementation of stringent SO_2 mitigation strategies.

The simulated and observed diurnal profiles of near-surface $PM_{2.5}$, O_3, NO_2, SO_2, and CO mass concentrations averaged over all monitoring sites in the GZB from 29 December 2018 to 29 January 2019 are showed in Fig. S2. The WRF-Chem model closely reproduces the diurnal variations of [$PM_{2.5}$] compared to observations. The MB and RMSE are 0.1 and 36.6 μg m^{-3}, respectively, and the IOA is 0.92. During the persistent haze episode, the model cannot satisfactorily replicate the several $PM_{2.5}$ peaks against observations. One of the most likely reasons is the uncertainty in the simulated meteorological fields, which determine the formation, transformation, diffusion, transport, and removal of air pollutants (Bei et al., 2012, 2013). The predicted O_3 and NO_2 diurnal variations are generally very consistent with observations, with IOA of 0.83 and 0.65, respectively. The model also yields reasonable predictions for SO_2 and CO temporal variations with IOA of 0.53 and 0.85, respectively. The deviations in SO_2 simulations are considerably large. A large fraction of SO_2 is emitted from power plants or agglomerated industrial zones, which can be regarded as point sources, so the transport of SO_2 is more sensitive to uncertainties in simulated wind fields. In addition to uncertainties in meteorological field simulations, uncertainties in emission inventory are also responsible for the model biases of air pollutants. Since implementation of the Air Pollution Prevention and Control Action Plan in 2013, strict emission control measures have been performed to improve the air quality, and the spatiotemporal variations in anthropogenic emissions in the GZB have changed considerably, which is not reflected in the emission inventory used in the present study (Li et al., 2017).

Figures S3a and b present the temporal profiles of measured and simulated sulfate, nitrate, and ammonium mass concen-

*The online version of this article can be found at https://doi.org/10.1007/s00376-020-0329-7.

Table S1. WRF-Chem model configurations.

Items	Configurations
Regions	East Asia
Study period	29 December 2018–29 January 2019
Domain size	200 × 200
Domain left	34.25°N, 119°E
Horizontal resolution	6 km × 6 km
Vertical resolution	35 vertical levels with a stretched vertical grid with spacing ranging from 30 m near the surface, to 500 m at 2.5 km and 1 km above 14 km
Microphysics scheme	WSM 6-class graupel scheme (Hong and Lim, 2006)
Boundary layer scheme	MYJ TKE scheme (Janjić, 2002)
Surface layer scheme	MYJ surface scheme (Janjić, 2002)
Land-surface scheme	Unified Noah land-surface model (Chen and Dudhia, 2001)
Longwave radiation scheme	Goddard longwave scheme (Chou et al., 2001)
Shortwave radiation scheme	Goddard shortwave scheme (Chou and Suarez, 1999)
Meteorological boundary and initial conditions	NCEP 1°×1° reanalysis data
Chemical initial and boundary conditions	MOZART 6-hour output (Horowitz et al., 2003)
Anthropogenic emission inventory	Developed by Zhang et al. (2009) and Li et al. (2017), 2013 base year, and SAPRC-99 chemical mechanism
Biogenic emission inventory	MEGAN model developed by Guenther et al. (2006)
Model spin-up time	4 days and 4 hours (Simulations starting time: 12:00 UTC on December 25, 2015)

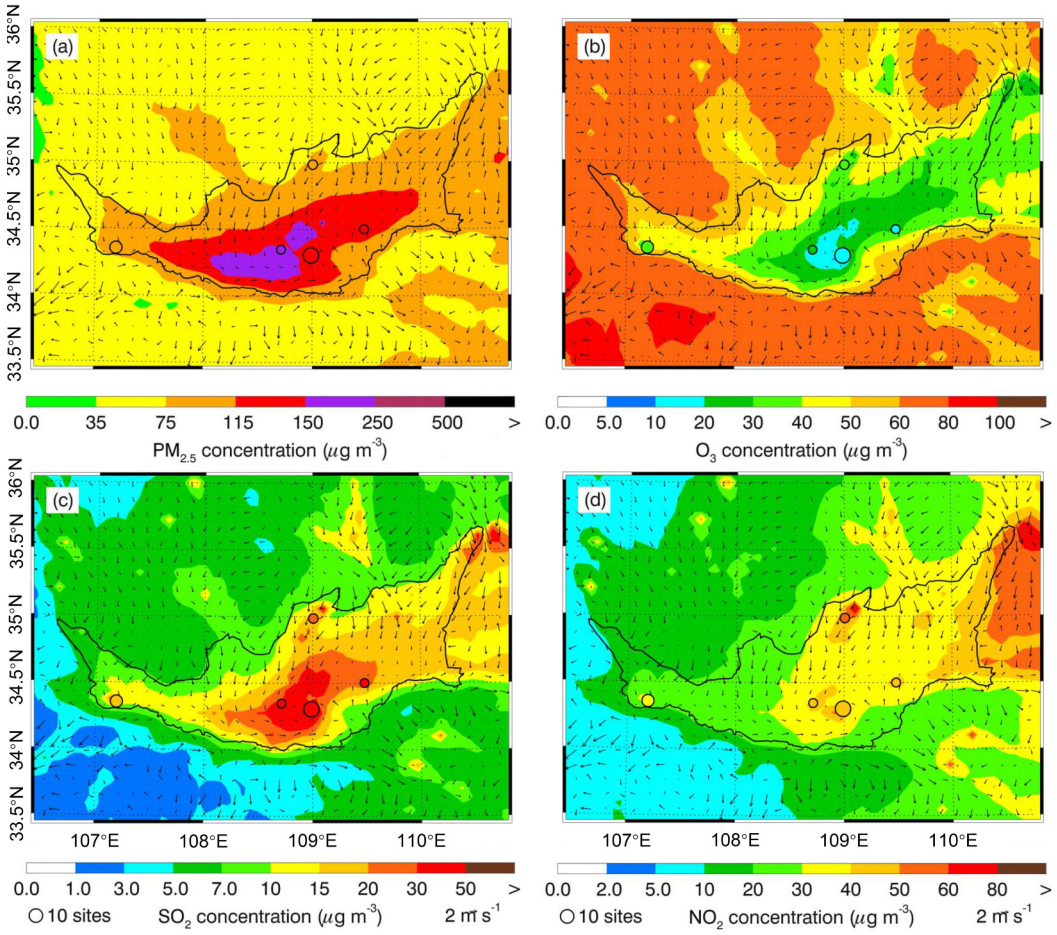

Fig. S1. Pattern comparisons of simulated (color counters) vs. observed (colored circles) near-surface mass concentrations of (a) $PM_{2.5}$, (b) O_3, (c) NO_2, and (d) SO_2 averaged from 29 December 2018 to 29 January 2019. The black arrows indicate simulated surface winds.

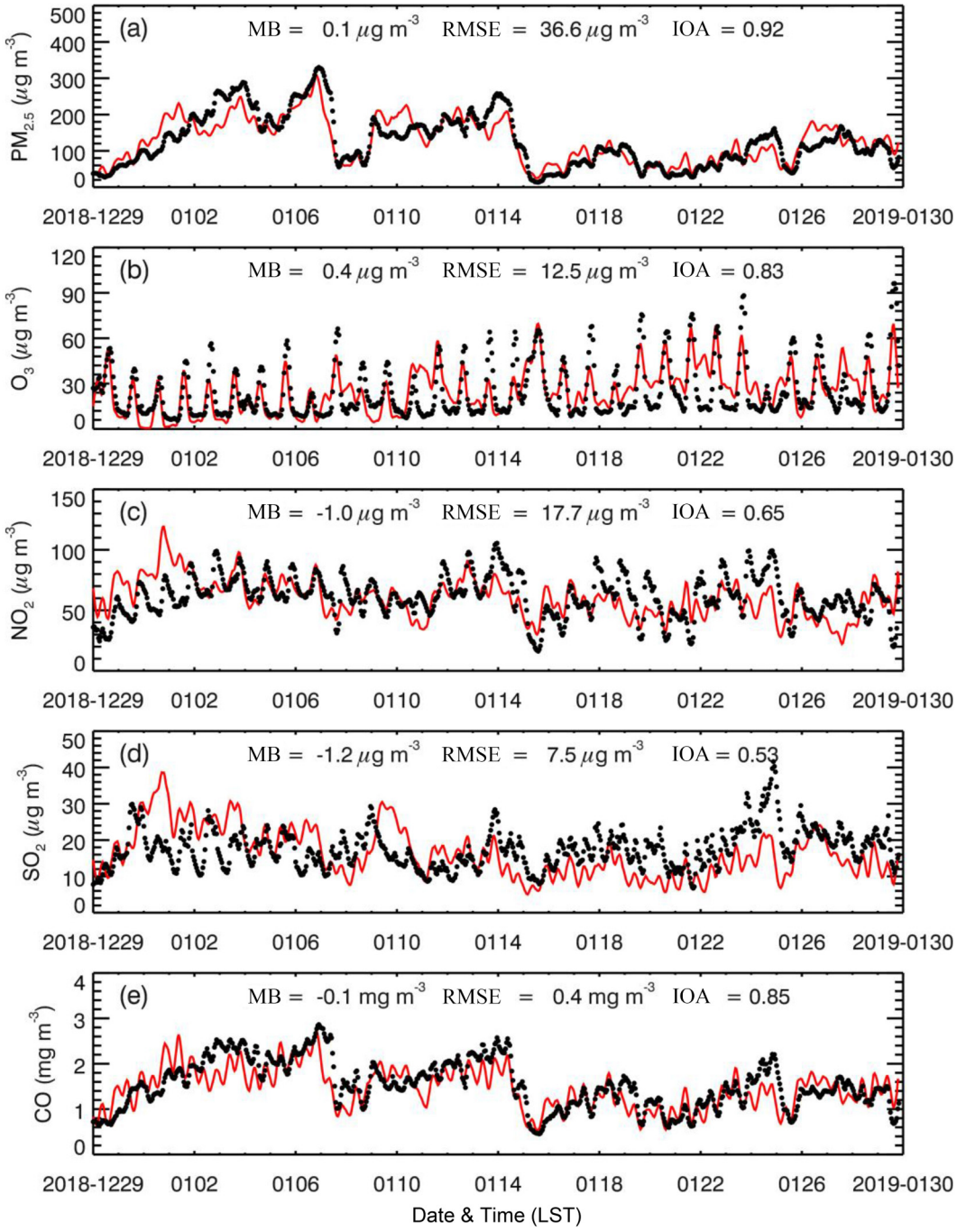

Fig. S2. Comparisons of observed (black dots) and simulated (solid red lines) diurnal profiles of near-surface hourly mass concentrations of (a) $PM_{2.5}$, (b) O_3, (c) NO_2, (d) SO_2, and (e) CO averaged over all ambient monitoring sites in the GZB from 29 December 2018 to 29 January 2019.

trations in Xianyang and Baoji, respectively. The simulated time series of sulfate, nitrate, and ammonium are generally in good agreement with measurements, with IOAs for nitrate and ammonium exceeding 0.80. Compared with nitrate and ammonium, the model biases are lager in sulfate simulations. Except for the anthropogenic SO_2 emissions and simulated meteorological fields, the SO_2 oxidation mechanism in the atmosphere also plays an important role in the sulfate simulation. In addition to direct emissions and SO_2 gas-phase oxidations by hydroxyl radicals and stabilized Criegee Intermediates (Liu et al., 2019), the SO_2 oxidation in aerosol water by O_2 catalyzed by Fe^{3+} is considered in the model simulations (Li et al., 2017). Recent studies have proposed that the aqueous oxidation of SO_2 by NO_2 under the condition of high relative humidity and NH_3 neutralization could interpret the efficient sulfate formation during wintertime haze events (Cheng et al., 2016; Wang et al., 2016; Liu et al., 2017). However, the mechanism is still not included in this study, which might further

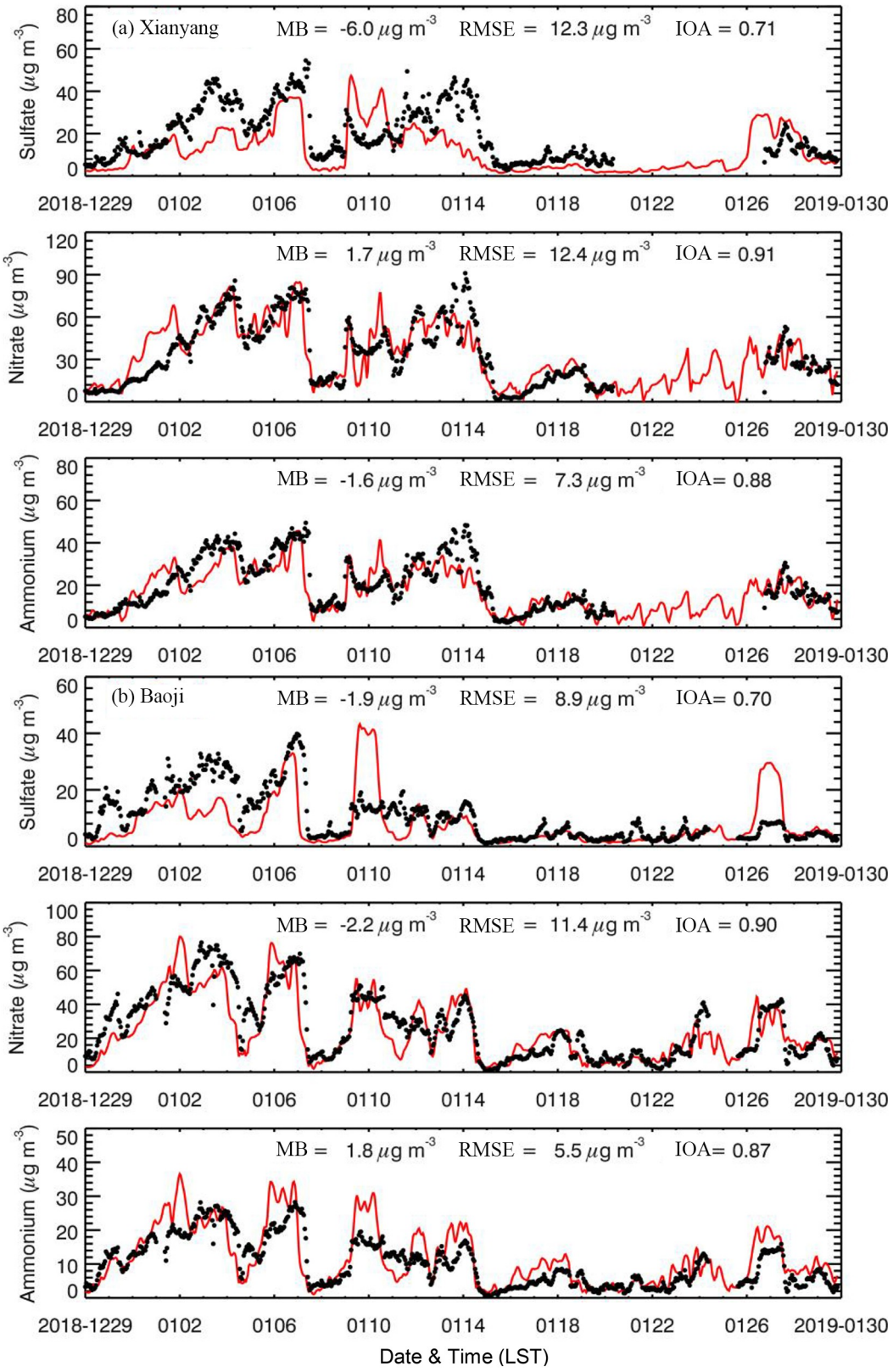

Fig. S3. Comparisons of observed (black dots) and simulated (solid red lines) diurnal profiles of sulfate, nitrate, and ammonium in (a) Xianyang and (b) Baoji from 29 December 2018 to 29 January 2019.

improve the sulfate simulation.

The good agreement of the simulated mass concentrations of air pollutants with observations at ambient monitoring

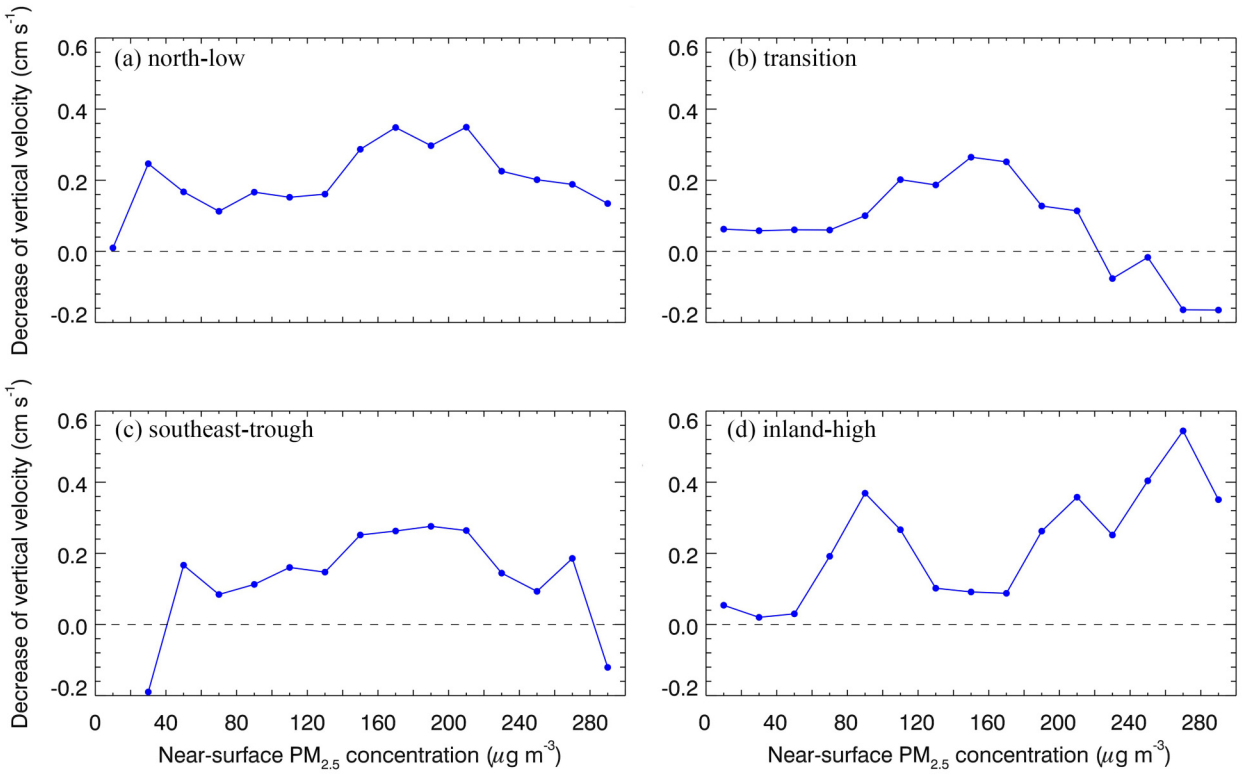

Fig. S4. Average decrease of the daytime updraft due to ARI as a function of the near-surface [$PM_{2.5}$] in the GZB under the synoptic pattern of (a) "north-low", (b) "transition", (c) "southeast-trough", and (d) "inland-high".

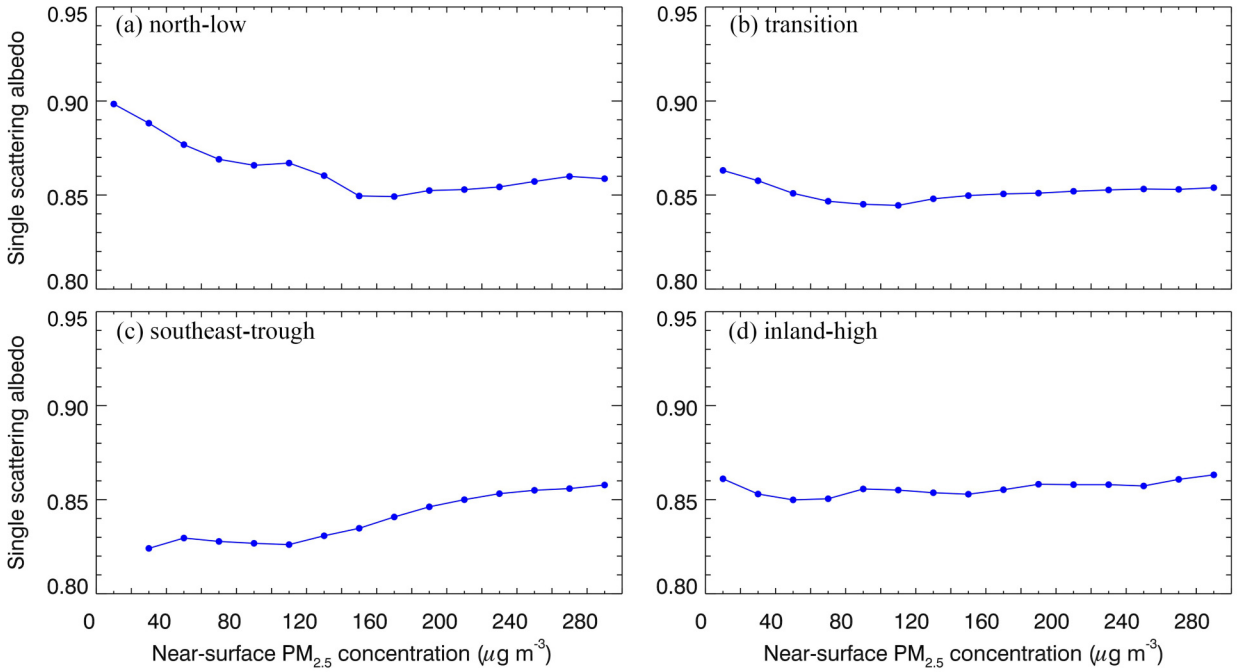

Fig. S5. Average variations of the daytime aerosol single scattering albedo as a function of the near-surface [$PM_{2.5}$] in the GZB under the synoptic pattern of (a) "north-low", (b) "transition", (c) "southeast-trough", and (d) "inland-high".

sites in the GZB and aerosol species with measurements in the two cities shows that the simulated meteorological fields and emission inventory used in the present study are generally reasonable, providing a reliable base for further evaluations.

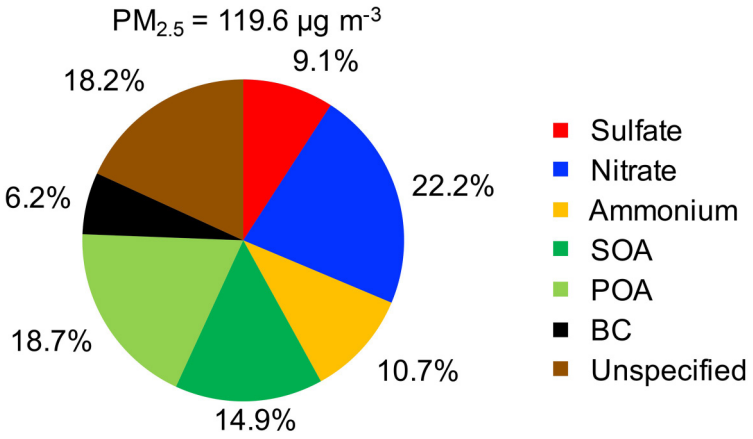

Fig. S6. Average chemical compositions of the near-surface $PM_{2.5}$ in the GZB form 29 December 2018 to 29 January 2019.

REFERENCES

Bei, N., G. Li, and L. T. Molina, 2012: Uncertainties in SOA simulations due to meteorological uncertainties in Mexico City during MILAGRO-2006 field campaign. *Atmospheric Chemistry and Physics*, **12**, 11 295–11 308, https://doi.org/10.5194/acp-12-11295-2012.

Bei, N. F., and Coauthors, 2013: Meteorological overview and plume transport patterns during Cal-Mex 2010. *Atmospheric Environment*, **70**, 477–489, https://doi.org/10.1016/j.atmosenv.2012.01.065.

Chen, F., and J. Dudhia, 2001: Coupling an advanced land surface-hydrology model with the Penn State-NCAR MM5 modeling system. Part I: Model implementation and sensitivity. *Monthly Weather Review*, **129**, 569–585, https://doi.org/10.1175/1520-0493(2001)129<0569:CAALSH>2.0.CO;2.

Cheng, Y. F., and Coauthors, 2016: Reactive nitrogen chemistry in aerosol water as a source of sulfate during haze events in China. *Science Advances*, **2**, e1601530, https://doi.org/10.1126/sciadv.1601530.

Chou, M. D., and M. J. Suarez, 1999: A solar radiation parameterization for atmospheric studies. NASA/TM-1999-104606.

Chou, M. D., M. J. Suarez, X. Z. Liang, and M. H. Yan, 2001: A thermal infrared radiation parameterization for atmospheric studies. NASA/TM-2001-104606.

Guenther, A., T. Karl, P. Harley, C. Wiedinmyer, P. I. Palmer, and C. Geron, 2006: Estimates of global terrestrial isoprene emissions using MEGAN (model of emissions of gases and aerosols from nature). *Atmospheric Chemistry and Physics*, **6**, 3181–3210, https://doi.org/10.5194/acp-6-3181-2006.

Hong, S. Y., and J. O. J. Lim, 2006: The WRF single-moment 6-class microphysics scheme (WSM6). *Asia-Pacific Journal of Atmospheric Sciences*, **42**, 129–151.

Horowitz, L. W., and Coauthors, 2003: A global simulation of tropospheric ozone and related tracers: Description and evaluation of MOZART, version 2. *J. Geophys. Res.*, **108**, 4784, https://doi.org/10.1029/2002JD002853.

Janjić, Z. I., 2002: Nonsingular implementation of the mellor-yamada level 2.5 scheme in the NCEP meso model. NCEP Office Note 437.

Li, M. M., T. J. Wang, M. Xie, B. L. Zhuang, S. Li, Y. Han, and P. L. Chen, 2017: Impacts of aerosol-radiation feedback on local air quality during a severe haze episode in Nanjing megacity, eastern China. *Tellus B*, **69**(1), 1339548, https://doi.org/10.1080/16000889.2017.1339548.

Liu, L., and Coauthors, 2019: Effects of organic coating on the nitrate formation by suppressing the N_2O_5 heterogeneous hydrolysis: A case study during wintertime in Beijing-Tianjin-Hebei (BTH). *Atmospheric Chemistry and Physics*, **19**, 8189–8207, https://doi.org/10.5194/acp-19-8189-2019.

Liu, M. X., and Coauthors, 2017: Fine particle pH during severe haze episodes in northern China. *Geophysical Research Letters*, **44**(10), 5213–5221, https://doi.org/10.1002/2017GL073210.

Wang, G. H., and Coauthors, 2016: Persistent sulfate formation from London Fog to Chinese haze. *Proceedings of the National Academy of Sciences of the United States of America*, **113**, 13 630–13 635, https://doi.org/10.1073/pnas.1616540113.

Zhang, Q., and Coauthors, 2009: Asian emissions in 2006 for the NASA INTEX-B mission. *Atmospheric Chemistry and Physics*, **9**, 5131–5153, https://doi.org/10.5194/acp-9-5131-2009.